New analogs of the clinical complement inhibitor compstatin with subnanomolar affinity and enhanced pharmacokinetic properties

Hongchang Qu[a], Daniel Ricklin[a], Hongjun Bai[a], Hui Chen[a], Edimara S. Reis[a], Mateusz Maciejewski[b], Apostolia Tzekou[a], Robert A. DeAngelis[a], Ranillo R. G. Resuello[c], Florea Lupu[d], Paul N. Barlow[b], John D. Lambris[a]

[a] Department of Pathology and Laboratory Medicine, University of Pennsylvania, Philadelphia, USA
[b] School of Chemistry and School of Biological Sciences, University of Edinburgh, United Kingdom.
[c] Simian Conservation Breeding and Research Center (SICONBREC), The Philippines.
[d] Cardiovascular Biology Research Program, Oklahoma Medical Research Foundation, USA

Supplementary Methods

Elucidation of Solution Structures

NMR sample and experiments. A 5-mM sample of compstatin analog Cp10 (Qu et al. 2011) was prepared at pH 4.0 in a buffer containing 10% D_2O, 10 mM acetic acid-d_4 (99.96%), and 0.01% NaN_3. The pH was adjusted with 0.1 M NaOH at 0.5 steps up to 6.0. At every step between pH 4.0 and 6.0 a 1D spectrum with a 3-9-19 water suppression block (Sklenář et al. 1993) was recorded at 10 ºC, with 32 scans and a 7212 Hz sweep width. It was observed that the positions of the peaks changed significantly. Therefore all further spectra for Cp10 were recorded at pH 6.0 in order to capture the more physiological conformation. At 15ºC, DQF-COSY, TOCSY (where the homonuclear relay of magnetization was afforded by an MLEV17 pulse train at a mixing time of 69.84 ms and power of 13.89 kHz) (Bax and Davis 1985) and NOESY spectra were recorded. Data collection entailed eight scans, 4096 by 2048 resolutions and 3-9-19 water suppression in case of DQF-COSY and TOCSY, and the same in case of NOESY but with a 3072 by 2048 resolution and a 300-ms mixing time. Additionally the NOESY spectrum for Cp10 was recorded on an 800-MHz Bruker NMR spectrometer with a cryogenic Z-gradient 5 mm TCI probe at a 9604 by 9604 Hz spectral width. All the other spectra were recorded on a 600-MHz Bruker NMR spectrometer equipped with a tri-axial gradient-capable 5 mm TXI probe, and at 7212 by 7212 Hz spectral widths.

The spectra were processed using the NMRPipe software (Delaglio et al. 1995) and analyzed using the Analysis software (v 2.1.5) obtained from the Collaborative Computing Project for the NMR community (Vranken et al. 2005). The assignments were achieved using standard methodology (Wuthrich 1986). The Analysis software was used to produce a peak volume-based table of assigned NOE signals in the ARIA format, where the lower distance limit was set to 2.2 Å and the upper distance limit to 5 Å, and in a few cases (very weak NOEs) to 6 Å. This list was then translated into the naming convention used in the Xplor-NIH software.

Calculation of NMR structures. For the structural calculations Xplor-NIH v. 2.24 was used (Schwieters et al. 2003). The analogs analyzed here contained unnatural amino acids not present in standard topology files used by the Xplor-NIH software. Therefore the existing CHARMM19 and CHARMM20 topology and parameter files that are typically used in the Xplor-NIH software were modified so as to make sure that sarcosine, side-chain N-methylated Trp and N-methylated Ile were correctly incorporated in the structure calculations. This was achieved by generation of appropriate unnatural amino acid CNS parameter and topology files using the PRODRG server (Schuttelkopf and van Aalten 2004) and further translation to the XPLOR standard. The structural calculation protocol started from generation of extended structures followed by initial minimization with all bonds broken. The next step was 10 ps of dynamics at 4000 K and then simulated annealing down to the temperature of 100 K in 5 K decrements, where each step was 1 ps long. Coordinates of each structure were finalized with 500 steps of Powell minimization. Throughout the calculation the van der Waals potential was introduced as a square potential well with a final force constant of 4 kcal mol^{-1} $Å^{-4}$. The NOE force constant was also set up as a square well with a force constant of 15 kcal mol^{-1} $Å^{-2}$. The angle, bond and improper angle potentials were instantiated as harmonic functions with final force constants standard for the CHARMM19 and CHARMM20 force fields.

Molecular dynamics. MD simulations of compstatin analogs 4W9A and Cp20 were performed using GROMACS 4.5.3 with periodic boundary conditions (Hess et al. 2008; Van der Spoel et al. 2005). The Gromos53a6 force field was applied with the missing parameter of mIle13 copied from residue mLeu of the force field. Residue Trp(Me)4 was replaced by Trp in Cp20 due to the lack of corresponding force field parameters for Trp(Me)4 and better comparability to analog 4W9A; since the MD analysis was focused on the core conformation, omission of this side chain methyl group is not expected to influence the result. Both 4W9A and Cp20 were solvated in a octahedron box (minimum boundary distance of 10 Å) using the SPC/E water model (Berendsen et al. 1987). Ions were added to neutralize the system and adjust the salt concentration close to physiological conditions (0.15 mol/L). The pressure was set to 1 atm using Parrinello-Rahman coupling (Parrinello and Rahman 1981), while the temperature was set to 300 K and controlled by the Berendsen thermostat (Berendsen et al. 1984). The bond length was constrained by LINCS method (Hess et al. 1997) allowing an integration step of 2 ps. Finally, the cut-off distance for van der Waals interactions was set to 14 Å, and electrostatic interactions were handled by the Particle-Mesh Ewald method (Darden et al. 1993; Essmann et al. 1995).

Computational analysis

AutoDock Vina(Trott and Olson 2010) was used for all docking studies that evaluated the binding to the compstatin binding site of C3c based on the co-crystal structure of analog 4W9A to C3c (Janssen et al. 2007). With exception of the backbone of the cyclic core region that can only be handled as rigid by Vina, all other parts of the peptides (terminal residues, side chains) were defined as flexible during the docking runs. The residues of C3c near the N-terminus of analog Cp20 (*i.e.*, Asp349, Lys386, Ser388, Asn390, Ser437, Asn452, Leu454, Asp491 and Leu492) were defined as flexible for the docking experiments in order to allow for more reasonable interactions between the extended N-terminus of these peptides and C3c. The only exception was peptide **19**, the N-terminus of which does not extend as other peptides; the binding site area on C3c therefore remained rigid in the docking of peptide **19**. Initial structures of all peptides were manually built in PyMol based on the C3c-bound structure of 4W9A. AutoDockTools was used to define the binding pocket and convert the initial structures of C3c and all peptides from the pdb format into the input format of Vina (pdbqt) (Sanner 1999). In the comparison plot of computational versus experimental binding free energy (ΔG), the experimental ΔG was calculated from the affinity values determined by SPR as $\Delta G = RT\ln(K_D)$, with R = 1.986 cal K^{-1} mol^{-1} and T = 293.15 K.

Analysis of compstatin plasma levels by UPLC-MS

Prior to analysis by UPLC-MS, compstatin analogs in the plasma samples were extracted by solid phase extraction (SPE) in a 96-well plate format (HLB Oasis 30 µm, 10 mg; Waters, Milford, MA). The SPE material was thoroughly conditioned using acetonitrile and water. Plasma samples were diluted 1:1 with 4% phosphoric acid, and a constant concentration of Cp20 (5 pM) was spiked into all samples containing peptides **3** or **14** as an internal standard; in the case of Cp20-containing samples, peptide **14** was used as internal standard. The samples were loaded on the SPE plate and washed with 10% acetonitrile in 0.1% formic acid. Extracted peptides were eluted with 200 µL of 65% acetonitrile in 0.1% formic acid and collected in a LoBind tube (Eppendorf) to avoid peptide adsorption. Finally, 5 µL of each eluent was diluted with 45 µL 0.1% formic acid and injected into the UPLC-MS system consisting of an online ACQUITY UPLC coupled to a SYNAPT G2-S HDMS instrument equipped with an ESI source and controlled by MassLynx 4.1 software (Waters). Each sample was injected in quadruplicates. Reversed-phase liquid chromatography was used for peptide separation with a 1.7 µm UPLC BEH130 C18 column (2.1 µm × 150 mm; Waters) at a column temperature of 40ºC. Peptides were separated at a flow rate of 0.15 mL/min with a linear gradient of 10–60% acetonitrile in water containing 0.1% formic acid over 8 min. Eluted peptides were directly analyzed by HDMS; the ESI source capillary voltage was set to 3.2 kV, the cone voltage to 30 V and the source temperature to 120ºC. [Glu1]-fibrinopeptide B (Sigma) was used for lock-mass correction with a sampling rate of 30 s. Mass spectra were acquired in positive mode over an m/z range of 50-1950 Da at a scan rate of 1 s.

Determination of C3 levels in NHP samples

The plasma concentration of C3 in individual cynomolgus monkeys used in this study was determined by ELISA. Briefly, 96-well plates (MaxiSorp; Nunc) were coated with 1 μg/ml of a monoclonal anti-C3 antibody (clone 8E11; kindly provided by Dr. Ronald Taylor, University of Virginia) (Tosic et al. 1989) in PBS overnight at 4ºC. Wells were washed with PBS/0.05% Tween and blocked with PBS/1% BSA for 1 h at room temperature. Plasma (diluted 1:10,000 and 1:20,000 in PBS/BSA) or serial dilutions of purified cynomolgus monkey C3 were then incubated for 1 h at room temperature followed by washing and incubation with peroxidase-conjugated anti-C3 (MP Biomedicals, Solon, OH) diluted 1:1,000 in PBS/BSA for 1 h at room temperature. The reaction was developed using tetramethylbenzidine substrate (R&D Systems, Minneapolis, MN) per manufacturer's instructions and optical density was determined using a microplate reader with wavelength set at 450 nm.

Supplementary References

Bax, A., Davis D.G., 1985. MLEV-17-based two-dimensional homonuclear magnetization transfer spectroscopy. J. Magn. Reson. 65, 355-360.

Berendsen, H.J.C., Grigera, J.R., Straatsma, T.P., 1987. The Missing Term in Effective Pair Potentials. J. Phys. Chem. 91, 6269-6271.

Berendsen, H.J.C., Postma, J.P.M., Vangunsteren, W.F., Dinola, A., Haak, J.R., 1984. Molecular-Dynamics with Coupling to an External Bath. J. Chem. Phys. 81, 3684-3690.

Darden, T., York, D., Pedersen, L., 1993. Particle Mesh Ewald - an N.Log(N) Method for Ewald Sums in Large Systems. J. Chem. Phys. 98, 10089-10092.

Delaglio, F., Grzesiek, S., Vuister, G.W., Zhu, G., Pfeifer, J., Ad Bax, A., 1995. NMRPipe: a multidimensional spectral processing system based on UNIX pipes. J. Biomol. NMR, 277-293.

Essmann, U., Perera, L., Berkowitz, M.L., Darden, T., Lee, H., Pedersen, L.G., 1995. A Smooth Particle Mesh Ewald Method. J. Chem. Phys. 103, 8577-8593.

Hess, B., Bekker, H., Berendsen, H.J.C., Fraaije, J.G.E.M., 1997. LINCS: A linear constraint solver for molecular simulations. J. Comput. Chem. 18, 1463-1472.

Hess, B., Kutzner, C., van der Spoel, D., Lindahl, E., 2008. GROMACS 4: Algorithms for highly efficient, load-balanced, and scalable molecular simulation. J Chem Theory Comput 4, 435-447.

Janssen, B.J., Halff, E.F., Lambris, J.D., Gros, P., 2007. Structure of compstatin in complex with complement component C3c reveals a new mechanism of complement inhibition. J. Biol. Chem. 282, 29241-29247.

Knerr, P.J., Tzekou, A., Ricklin, D., Qu, H., Chen, H., van der Donk, W.A., Lambris, J.D., 2011. Synthesis and activity of thioether-containing analogues of the complement inhibitor compstatin. ACS Chem. Biol. 6, 753-760.

Parrinello, M., Rahman, A., 1981. Polymorphic Transitions in Single-Crystals - a New Molecular-Dynamics Method. J. Appl. Phys. 52, 7182-7190.

Qu, H., Magotti, P., Ricklin, D., Wu, E.L., Kourtzelis, I., Wu, Y.Q., Kaznessis, Y.N., Lambris, J.D., 2011. Novel analogues of the therapeutic complement inhibitor compstatin with significantly improved affinity and potency. Mol. Immunol. 48, 481-489.

Sanner, M.F., 1999. Python: A programming language for software integration and development. J. Mol. Graphics Model. 17, 57-61.

Schuttelkopf, A.W., van Aalten, D.M., 2004. PRODRG: a tool for high-throughput crystallography of protein-ligand complexes. Acta Crystallogr. Sect. D. Biol. Crystallogr. 60, 1355-1363.

Schwieters, C.D., Kuszewski, J.J., Tjandra, N., Clore, G.M., 2003. The Xplor-NIH NMR molecular structure determination package. J. Magn. Reson. 160, 65-73.

Sklenář, V., Piotto, M., Leppik, R., Saudek, V., 1993. Gradient-Tailored Water Suppression for 1H-15N HSQC Experiments Optimized to Retain Full Sensitivity. J. Magn. Reson. Imaging 102, 241-245.

Tosic, L., Sutherland, W.M., Kurek, J., Edberg, J.C., Taylor, R.P., 1989. Preparation of monoclonal antibodies to C3b by immunization with C3b(i)-sepharose. J. Immunol. Methods 120, 241-249.

Trott, O., Olson, A.J., 2010. AutoDock Vina: improving the speed and accuracy of docking with a new scoring function, efficient optimization, and multithreading. J. Comput. Chem. 31, 455-461.

Van der Spoel, D., Lindahl, E., Hess, B., Groenhof, G., Mark, A.E., Berendsen, H.J.C., 2005. Gromacs: Fast, Flexible, and Free. J. Comput. Chem. 26, 1701-1718.
Vranken, W.F., Boucher, W., Stevens, T.J., Fogh, R.H., Pajon, A., Llinas, M., Ulrich, E.L., Markley, J.L., Ionides, J., Laue, E.D., 2005. The CCPN data model for NMR spectroscopy: development of a software pipeline. Proteins 59, 687-696.
Wuthrich, K. 1986. NMR of Proteins and Nucleic Acids. Wiley, John & Sons, Incorporated, New York.

Supplementary Tables and Figures

New analogs of the clinical complement inhibitor compstatin with subnanomolar affinity and enhanced pharmacokinetic properties

Hongchang Qu[a,1,2], Daniel Ricklin[a,1], Hongjun Bai[a], Hui Chen[a], Edimara S. Reis[a], Mateusz Maciejewski[b], Apostolia Tzekou[a], Robert A. DeAngelis[a], Ranillo R. G. Resuello[c], Florea Lupu[d], Paul N. Barlow[b], John D. Lambris[a,*]

[a] Department of Pathology and Laboratory Medicine, University of Pennsylvania, Philadelphia, USA
[b] School of Chemistry and School of Biological Sciences, University of Edinburgh, United Kingdom.
[c] Simian Conservation Breeding and Research Center (SICONBREC), The Philippines.
[d] Cardiovascular Biology Research Program, Oklahoma Medical Research Foundation, USA

Table of Content

Supp. Fig. 1:	NMR peaks identifying unique structural features of Cp10	S2
Supp. Table 1:	Statistics of Cp10 structure calculations	S2
Supp. Fig. 2:	Structural comparison between Cp10, 1A1P and 2QKI	S3
Supp. Fig. 3:	Molecular dynamics simulation of Cp20 and 4W9A	S4
Supp. Fig. 4:	SPR sensorgrams of peptides **1-20**	S5
Supp. Fig. 5:	Correlation between calculated and experimental DG values	S6
Supp. Fig. 6:	UPLC retention time of selective peptides	S6
Supp. Table 2:	Plasma C3 concentrations of cynomolgus monkeys	S7
Supp. Fig. 7:	Analogue binding to human and NHP C3 (SPR analysis)	S7
Supp. Fig. 8:	Sequence alignment between human and NHP C3	S8

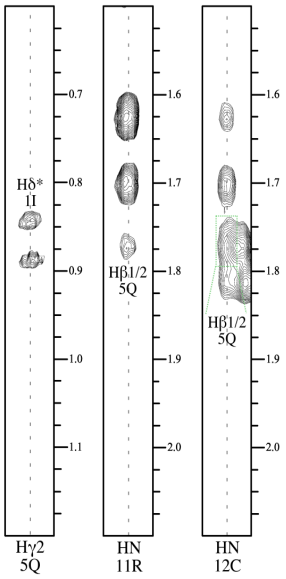

Supplementary Figure 1. Strips presenting peaks that identify unique structural features of Cp10. The 5Q $H_{\gamma 2}$ – 11$H_{\delta *}$ distance in the solution (PDB 1A1P) and bound form (PDB 2QKI) is 14.7 Å and 12.3 Å, respectively. The 11R H_N – 5Q Hβ1/2 distance in 1A1P and 2QKI is 8.8 Å and 6.6 Å, respectively. The 12C HN – 5Q $H_{\beta 1/2}$ distance in 1A1P and 2QKI is 12.1 Å and 6.6 Å, respectively.

Supplementary Table 1. Statistics of Cp10 structure calculations based on lowest energy 20 structures. In the NOE break-down, the number of NOEs considered is shown in the parentheses.

	Cp10
RMS deviation from ideal geometry	
Angle [º]	0.74 ± 0.17
Bond [Å]	0.007 ± 0.001
Improper [º]	0.40 ± 0.11
RMS deviation of NOEs	
Intra-residue	(118) 0.131 +/- 0.002
Sequential	(42) 0.141 +/- 0.002
Mid range	(22) 0.178 +/- 0.016
Long range	(22) 0.174 +/- 0.006
Total	(204) 0.144 +/- 0.001
Coordinate precision [Å]	
Heavy backbone atoms	0.04
All atoms	0.43

A

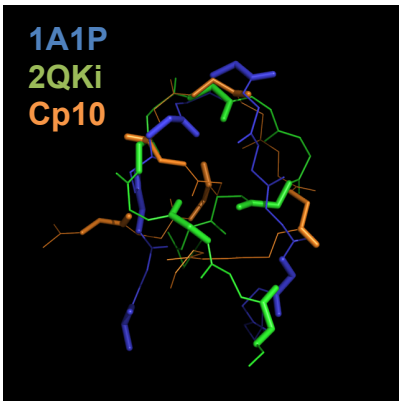

B

1A1P: Ac-Ile-[Cys-Val-Val -Gln-Asp-Trp-Gly-His-His-Arg-Cys]-Thr-NH_2
2QKI: Ac-Ile-[Cys-Val-Trp(Me)-Gln-Asp-Trp-Gly-Ala-His-Arg-Cys]-Thr-NH_2
Cp10: Ac-Ile-[Cys-Val-Trp(Me)-Gln-Asp-Trp-Sar-Ala-His-Arg-Cys]-Ile-NH_2

C

[RMSD]	1A1P (free)	2QKI (bound)
1A1P	-	3.7
Cp10	3.4	4.3

D

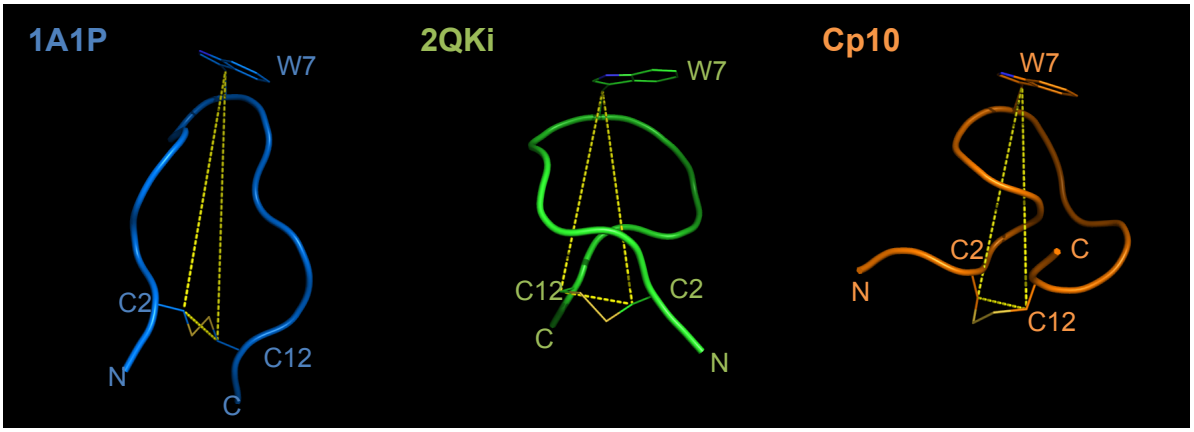

E

[Å]	C2-C12	C2-W7	W7-C12
1A1P	4.6	14.3	15.2
2QKI	3.9	12.3	11.8
Cp10	3.4	12.1	12.9

Supplementary Figure 2. Conformational arrangement of Cp10 (NMR structure; lowest-energy conformer) in comparison with the available structures of free compstatin (PDB 1A1P) and C3c-bound analog 4W9A (PDB 2QKI). (A-C) The backbone atoms (n+ca+c) of the conserved residues I1, V3, Q5, W7 and H10 (B; shown as sticks in the superimposition in panel A) were used to calculate the RMSD of the backbone shown in panel C. (D-E) Ribbon representation of free compstatin (left), bound analog 4W9A (middle) and the NMR structure of Cp10 (right) with residues C2, W7, and C12 shown as lines using the same relative orientation and zoom level (D). The distances between the βC atoms of the three residues are highlighted as yellow dashed lines and listed in the table in panel E.

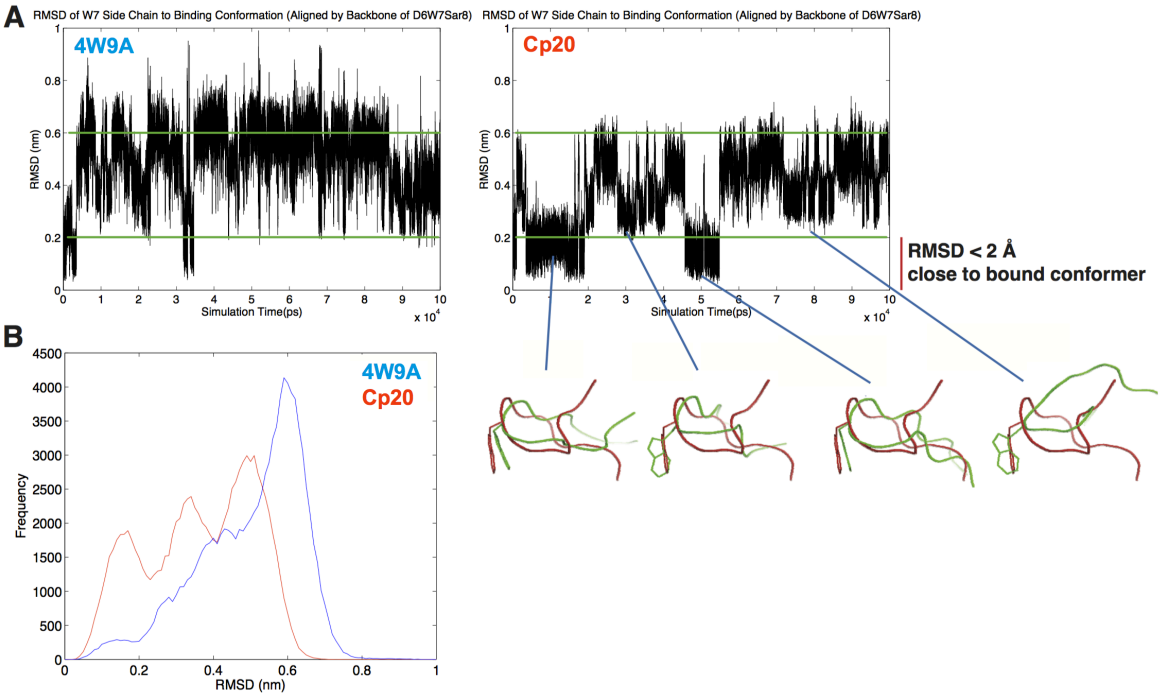

Supplementary Figure 3. Molecular dynamics simulation of conformational states in analogs 4W9A and Cp20 over a period of 100 ns. (A) Local conformations as measured by RMSD between the simulated and C3c-bound orientation of Trp7. Green lines mark states that represent more open (RMSD ~ 0.6 nm) and bound-like states (RMSD ~ 0.2 nm). Structural snapshots of the simulated Cp20 conformation (green) at various time points are shown superimposed with the bound conformer (red) and represented as a ribbon with Trp7 shown as sticks. (B) Relative distribution of conformational states between the two analogs.

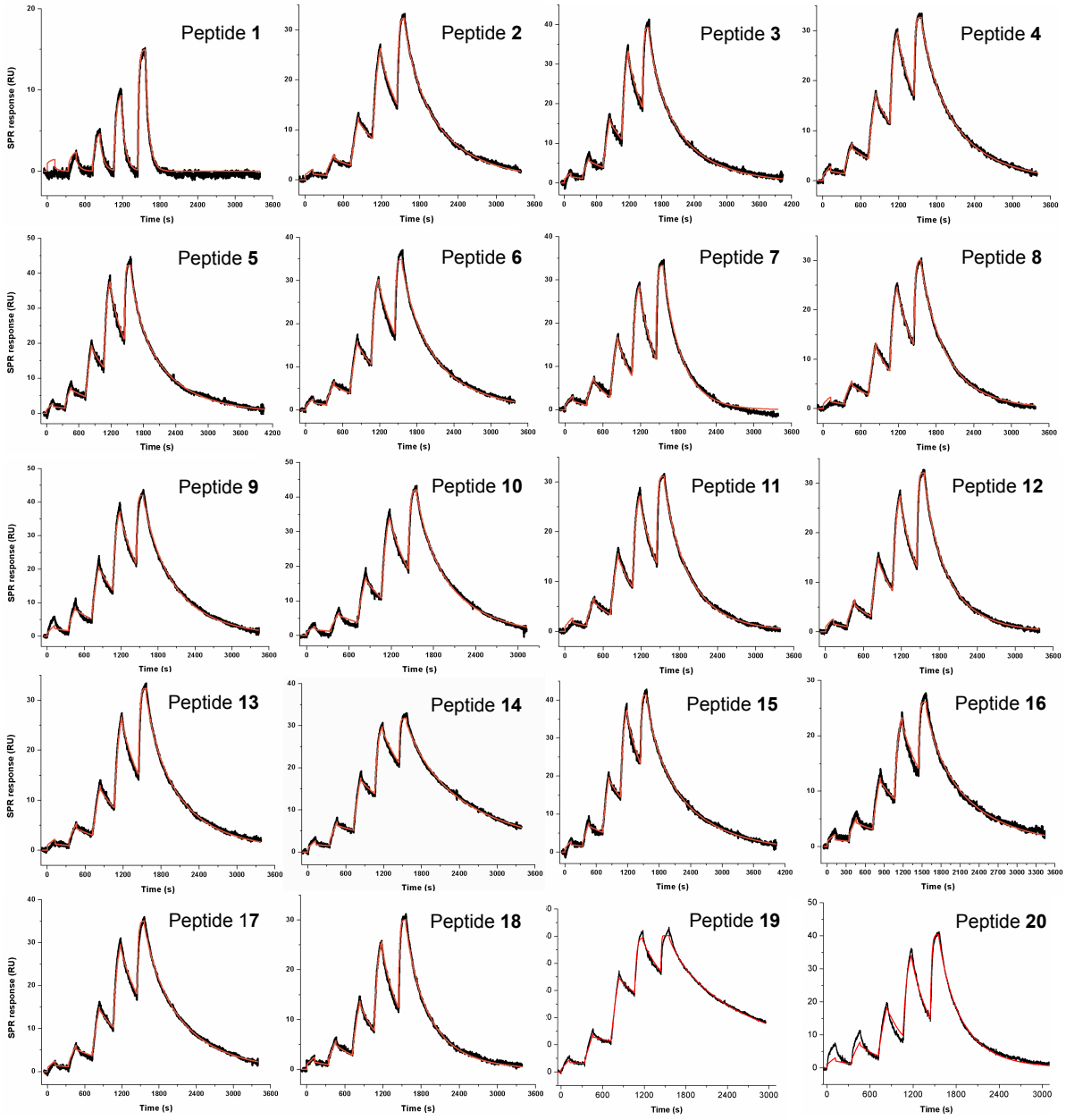

Supplementary Figure 4. Kinetic analysis of peptides **1-20** as listed in Table 1. Each SPR sensorgram represents a single cycle kinetic titration of an individual peptide over 5 concentrations (black: processed SPR data; red: kinetic fit to 1:1 Langmuir model).

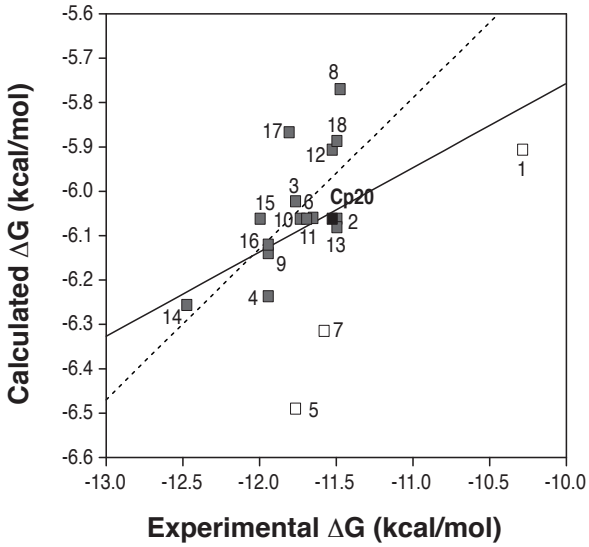

Supplementary Figure 5. Correlation between free energy values (ΔG) as calculated from the docking experiment (y axis; AutoDock score) and from the experimentally determined affinity values (x axis). Peptide numbers are shown next to each mark on the plot. The correlation over the entire data set is shown as a solid line whereas the dotted line represents the correlation after exclusion of peptides **1**, **5** and **7**.

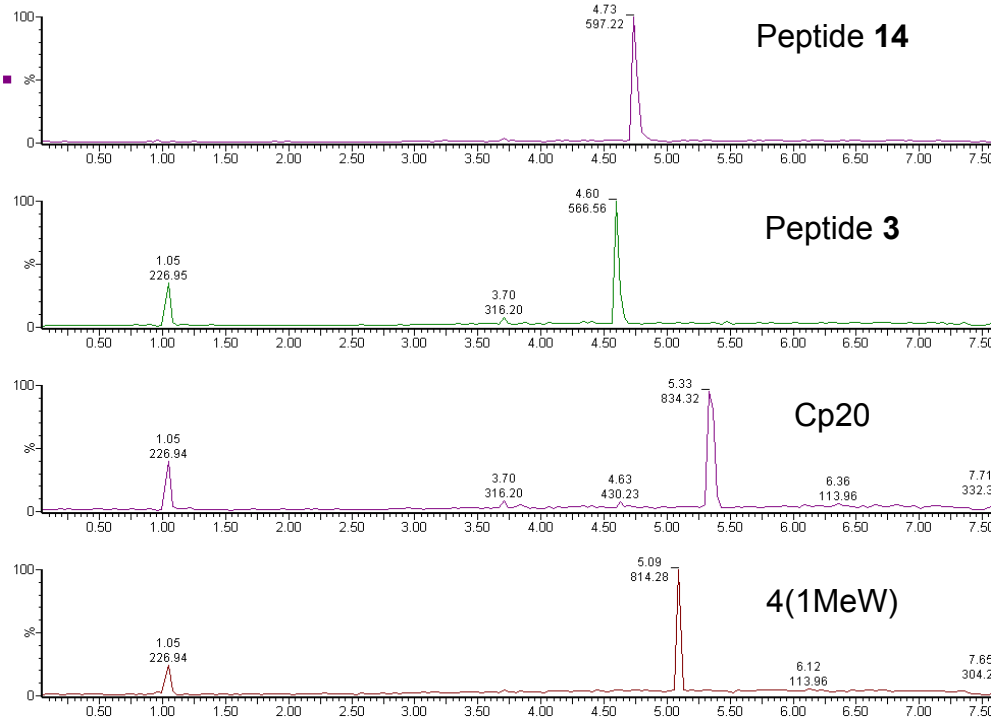

Supplementary Figure 6. UPLC retention time of selective peptides (from top to bottom: peptide **14**, peptide **3**, Cp20, 4(1MeW)).

Supplementary Table 2. Plasma C3 concentrations of cynomolgus monkeys involved in the pharmacokinetic assessment.

Animal	#1	#2	#3	#4	#5	#6
Body Weight	3.2	3.2	3.4	3.5	3.1	3.2
Compound	Cp20	Cp20	Peptide **3**	Peptide **3**	Peptide **14**	Peptide **14**
Dose (mg/kg)	2.0	2.0	2.0	2.0	2.0	2.0
C3 Conc. (mg/ml)	0.9	1.2	1.5	1.2	2.0	2.3
C3 Conc. (µM)	4.6	6.3	8.0	6.3	10.7	12.4

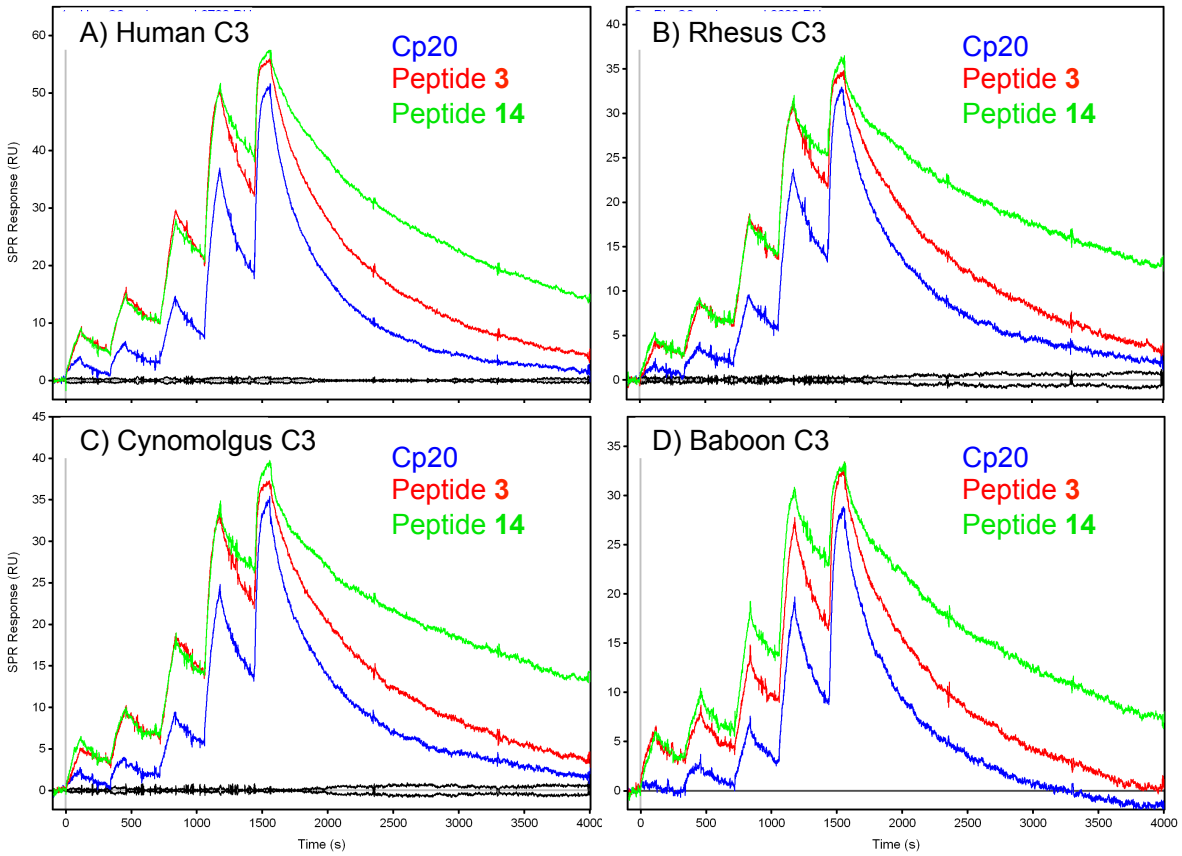

E)

	Cp20	Peptide **3**	Peptide **14**
Human	1.00	1.00	1.00
Rhesus	0.75	0.89	0.69
Cynomolgus	0.85	0.95	0.73
Baboon	0.98	0.93	0.77

Supplementary Figure 7. Comparative screening of various compstatin analogs to C3 from human, baboon, cynomolgus monkey and rhesus monkey plasma using SPR single cycle kinetics titration. (A-D) Superimposed sensorgrams of Cp20, peptide **3** and peptide **14** per C3 species (note that the concentration range for peptide 3 was 0.9–73 nM in panels A-C; all other injections were performed at 0.5–40 nM). (E) Relative binding affinities (calculated based on kinetic fitting to a 1:1 Langmuir binding model relative to human C3 on the same sensor chip).

A

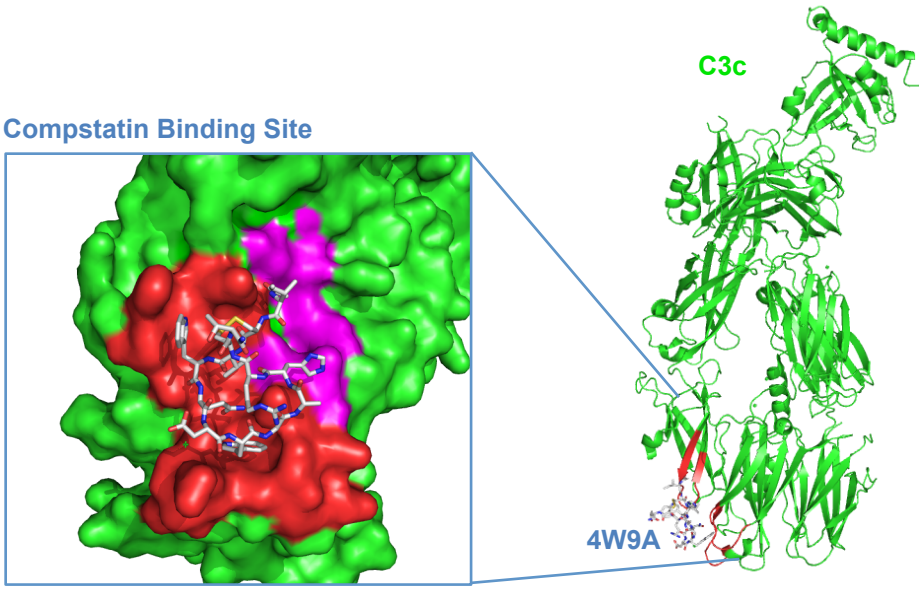

B

```
301  VLSRKVLLDGVQNPRAEDLVGKSLYVSATVILHSGSDMVQAERSGIPIVTSPYQIHFTKT  360  P01024  Human
301  VLSRKVLLDGVQNPRPEDLVGKSLYVSVTVILHSGSDMVQAERSGIPIVTSPYQIHFTKT  360  G7PYU9  Cynomolgus
301  VLSRKVLLDGVQNPRPEDLVGKSLYVSVTVILHSGSDMVQAERSGIPIVTSPYQIHFTKT  360  G7NML7  Rhesus
     *************** ***********.********************************

361  PKYFKPGMPFDLMVFVTNPDGSPAYRVPVAVQGEDTVQSLTQGDGVAKLSINTHPSQKPL  420  P01024  Human
361  PKYFKPGMPFDLMVFVTNPDGSPAYRVPVAVQGEDAVQSLTQGDGVAKLSINTHPSQKPL  420  G7PYU9  Cynomolgus
361  PKYFKPGMPFDLMVFVTNPDGSPAYRVPVAVQGEDAVQSLTQGDGVAKLSINTHPSQKPL  420  G7NML7  Rhesus
     ************************************:***********************

421  SITVRTKKQELSEAEQATRTMQALPYSTVGNSNNYLHLSVLRTELRPGETLNVNFLLRMD  480  P01024  Human
421  SITVRTKKRELSEAEQATRTMEAQPYSTVGNSNNYLHLSVPRAELRPGETLNVNFLLRMD  480  G7PYU9  Cynomolgus
421  SITVRTKKRELSEAEQATRTMEAQPYSTVGNSNNYLHLSVPRAELRPGETLNVNFLLRMD  480  G7NML7  Rhesus
     ********:************:* **************** *:******************

481  RAHEAKIRYYTYLIMNKGRLLKAGRQVREPGQDLVVLPLSITTDFIPSFRLVAYYTLIGA  540  P01024  Human
481  RTQEAKIRYYTYLIMNKGKLLKVGRQVREPGQDLVVLPLSITTDFIPSFRLVAYYTLIGA  540  G7PYU9  Cynomolgus
481  RTQEAKIRYYTYLIMNKGKLLKVGRQVREPGQDLVVLPLSITTDFIPSFRLVAYYTLIGA  540  G7NML7  Rhesus
     *::****************:***.************************************

541  SGQREVVADSVWVDVKDSCVGSLVVKSGQSEDRQPVPGQQMTLKIEGDHGARVVLVAVDK  600  P01024  Human
541  NGQREVVADSVWVDVKDSCVGSLVVKSGQSEDRQPLPGQQMTLKIEGDHGARVGLVAVDK  600  G7PYU9  Cynomolgus
541  NGQREVVADSVWVDVKDSCVGSLVVKSGQSEDRQPLPGQQMTLKIEGDHGARVGLVAVDK  600  G7NML7  Rhesus
     .************************************:***************** ******
```

Supplementary Figure 8. Sequence similarity in the compstatin binding site region of human and selected NHP in C3c. (A) Residues comprising the binding region of analog 4W9A (stick representation) and the extended binding patch potentially targeted by peptides 3 and 14 (magenta) on C3c (green cartoon) are highlighted in red. The box shows a closeup view of the binding site. (B) Sequence alignment between C3 from humans (UniProt entry P01024), cynomolgus monkeys (Macaca fascicularis; UniProt entry G7PYU9) and rhesus monkeys (Macaca mullata; UniProt entry G7NML7) shows a high degree of identical (*), conserved (:) or semi-conserved (.) residues, including in the binding areas of compstatin analogs (red/magenta). Only residues 301-600 of each entry are shown in this alignment. No genomic data for baboons are available in UniProt (www.uniprot.org).